# Changes in the Chemical Structure and Properties of a Perfluorosulfonated Acid Membrane Induced by Fuel-Cell Operation

**C. Bas,[1] L. Flandin,[1] A.-S. Danerol,[1] E. Claude,[2] E. Rossinot,[2] N. D. Alberola[1]**

[1]*Laboratoire Matériaux Organiques à Propriétés Spécifiques (Unité Mixte de Recherche 5041, Centre National de la Recherche Scientifique), Université de Savoie, Campus Scientifique, Bâtiment IUT, 73376 Le Bourget du Lac Cedex, France*
[2]*Axane, 2 Rue de Clémencière, BP15, 38360 Sassenage, France*

Received 27 March 2009; accepted 30 August 2009
DOI 10.1002/app.31386
Published online 7 April 2010 in Wiley InterScience (www.interscience.wiley.com).

**ABSTRACT:** Changes in a perfluorosulfonated acid polymer membrane in membrane electrode assemblies were studied after different times under stationary conditions in fuel cells. A large series of characterizations demonstrated changes in the morphology, mechanical behavior, and thermal stability upon aging. Overall, the membrane evolution could be mainly attributed to both chemical degradation and cationic contamination. The reduction in the membrane thickness, detected by scanning electron microscopy, was ascribed to a radical unzipping mechanism and polymer chain erosion after 900 h in service. An additional monotonic decrease in the number of $C_{tertiary}F$ groups was observed even at 400 h. In parallel, membranes were cation-contaminated, and this led to drastic changes in the thermal and mechanical properties in the first stage of fuel-cell operation. The pollution cations were shown to have Lewis acid strengths close to 0.25 and thus strongly interacted with sulfonate anions of the membrane. The kinetic dependence of these membrane modifications and the influence of the platinum band were also examined.
 J Appl Polym Sci 117: 2121–2132, 2010

**Key words:** ageing; degradation; ionomers; polyelectrolytes

## INTRODUCTION

Proton-exchange membrane fuel cells are an important industrial issue for many applications because they can directly convert chemical energy into electrical energy. However, their performance stability under normal service conditions remains a major drawback for their commercialization. It is well known that the performance of fuel cells closely depends on the characteristics of the membrane electrode assembly (MEA), a key component of the system. The MEA is a multilayered structure based on a polymer membrane acting as a solid electrolyte, coated on both sides by active layers (anode and cathode layers), and covered by gas diffusion layers. As one of the predominant failure modes of polymer electrolyte membrane fuel cells originates from the lifetime of the polyelectrolyte, many articles have examined the degradation of the membrane.[1,2] Good candidates for the polymer membrane within MEAs for proton-exchange membrane fuel-cell applications are perfluorinated sulfonic acid (PFSA) membranes and especially the most famous one, Nafion ionomer. Many authors have pointed out that the PFSA membrane degradation process can be described as an unzipping mechanism due to carboxylic acid end groups reaction with hydroxyl radicals[3,4] (Scheme 1). This mechanism has also been proposed when the unzipping reaction of the main-chain end group approaches the junction with the side chain (Scheme 2). This mechanism is supported by chemical analyses of fuel-cell outlet water (e.g., HF ions,[5–11] sulfate ions,[9,11–13] different perfluorinated carboxylic acids,[3,13] and hydrogen peroxide and its radicals[11,14–18]). The unzipping degradation mechanism induces no chemical modification within the membrane. The last stage of this degradation appears as a decrease in the thickness.[19] Nevertheless, recent work performed by Xie and Hayden[4] revealed an increase in IR carbonyl absorption bands within the membrane with the aging time. This band, related to carboxylic acid groups, implied that cleavage could occur in the side chain. Nevertheless, others articles have reported that the degradation predominantly takes place in the side chains.[20,21] In addition, other chemical modifications of the membrane with respect

*Correspondence to:* C. Bas (corine.bas@univ-savoie.fr).
Contract grant sponsors: Region Rhône-Alpes (through a doctoral fellowship to A.-S.D.).

$$-CF_2COOH + 2\,OH^{\circ} \rightarrow -COOH + CO_2 + 2\,HF$$

**Scheme 1** Chemical balance of the degradation propagation mechanism.[3,4]

to the pendent chain have been detected by Fourier transform infrared (FTIR) spectroscopy at about 1460 and 870 $cm^{-1}$. The first FTIR band is related to the S=O stretching mode[9,22–24] and has been attributed to either $SO_2F$ or $SO_2$—O—$SO_2$ groups. This last hypothesis could suggest some reticulation process implying sulfonic units. The second band could be related to O—O or Fe—O—Fe moieties.[23] However, these additional chemical changes were observed by FTIR only after accelerated durability tests, particularly the Fenton test, even without an iron catalyst.

In this work, the microstructural evolution of PFSA membranes after fuel-cell operation upon stationary solicitation was investigated with tensile testing, dynamic mechanical analysis (DMA), and thermogravimetric analysis (TGA). Correlations with chemical analyses such as solid-state $^{19}F$-NMR and ion-exchange capacity (IEC) measurements were performed. This study was focused on three-layer sample experiments (i.e., active layer/membrane/active layer).

## EXPERIMENTAL

### Materials

As-received and aged MEAs, industrially produced, were provided by Axane Co. (Sassenage, France) The MEAs were multilayered structures based on PFSA polymer films coated on both sides by active layers and covered by gas diffusion layers (carbon cloth). The polymer membrane was an extruded PFSA with an IEC of 0.9. The electrodes were composed of a porous, carbon-supported, nanosized platinum catalyst with an ionomer binding agent showing a chemical structure similar to that of the polymer electrolyte. The so-called as-received MEAs were never mounted in a stack; they thus were never subjected to mechanical stresses upon cell assembly. The so-called aged MEAs were tested in a 55-cell stack system at 60°C in a constant-power-mode system (0.18 A/$cm^2$ and 0.67 V) for several life test durations: 347, 892, and 1397 h. The anode side was fed pure humidified hydrogen (1.2 bar), whereas the cathode side received humidified air (75% relative humidity) at atmospheric pressure. The gas flow rates were 5 and 30 NL/min for $H_2$ and air, respectively. As the characterization was focused on electrode-coated membranes, the gas diffusion layers were first removed from the MEAs without any damage to the electrodes because of the low adhesion to the carbon cloth due to the manufacturing of the carbon-coated membrane. In addition, investigations were performed on nonregenerated and regenerated membranes in an acid form. To this end, pieces of electrodes membrane assemblies were first soaked in a 50% ethanol/50% deionized water solution for 1 h in an ultrasonic bath to remove electrodes and then were washed in deionized water. Then, these nonregenerated membranes were immersed in HCl (37%) for 1 h in an ultrasonic bath. At last, the membranes were washed in deionized water to remove excess acid. The resulting membranes were defined as regenerated membranes.

### Experimental procedures for the membranes

#### Scanning electron microscopy (SEM)

Morphological analyses of electrode-coated membranes were performed with the help of a Leica Stereoscan 440 scanning electron microscope (Cambridge Ltd., England) at a 20-kV accelerating voltage in the backscattered mode. Small pieces of the electrode-coated membranes were embedded in an epoxy resin at the ambient temperature, and then the sample cross sections were carefully polished and metalized before testing.

#### Tensile tests

The electrode-coated membranes were cut into standard dog-bone samples with a gauge length of 2.2 cm and a width of 0.5 cm (NF ISO 6239). Uniaxial tensile tests were performed with an Adamel

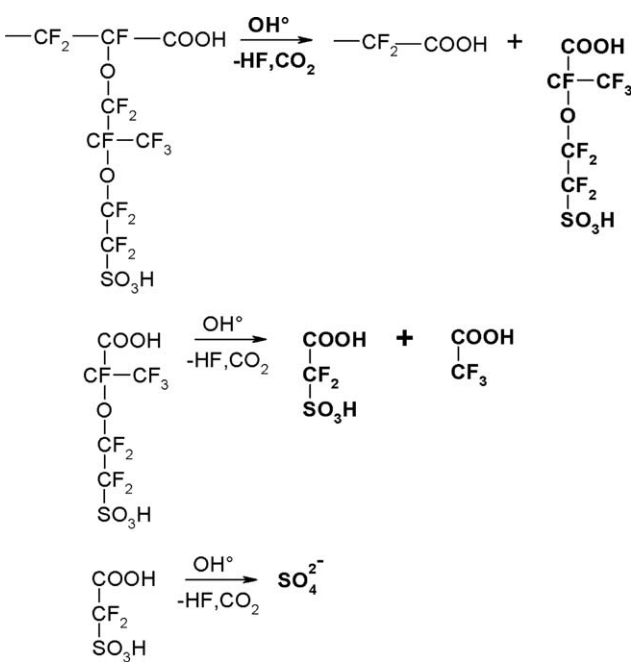


**Scheme 2** Degradation processes involving side chains.[3,4] Products in bold were detected in the fuel-cell outlet water.[3,5–18]

Lhomargy (Ivry sur Seine, France) tensile machine at the ambient temperature (23 ± 1°C) with controlled humidity (50–60%) at a crosshead speed of 5 mm/min. As the specimens were composites with fragile electrode coatings, the stress was estimated with only the membrane thicknesses (ca. 0.03 mm) and not the overall thickness of the electrode-coated membranes (0.05 mm). The average values of Young's modulus ($E$), the yield stress or stress at break, and the strain at break were determined from load–deformation curves of five tensile measurements. $E$ was calculated from the initial slope of the stress–strain plot.

### Dynamic mechanical thermal analysis (DMTA)

DMA was performed on as-received and aged electrode-coated membranes. Measurements were performed with a Polymer Laboratories DMTA MKII spectrometer (Loughborough, UK) operating in the tensile mode. This apparatus provided the real and imaginary parts of the dynamic mechanical modulus, that is, the storage modulus ($E'$) and the loss modulus ($E''$), respectively. The mechanical damping ($\tan \delta = E''/E'$) was also calculated. $E'$, $E''$, and $\tan \delta$ were displayed as functions of temperature for 1, 3, and 10 Hz under isochronal conditions. Isochronal scans were recorded from the ambient temperature to 400°C at a heating rate of 1°C/min under a dry nitrogen flow to limit polymer oxidation. Before the tests, MEA pieces were dried under a nitrogen gas flow for at least 1 h. From the $E'$–temperature curve, the onset temperature of the drop modulus ($T_{onset\text{-}DMTA}$) and the temperature of the $\alpha$ relaxation ($T_\alpha$) could be determined as the temperature from which $E'$ strongly decreased and as the temperature at the maximum of the damping factor, respectively.

### Coupled TGA

Thermal degradation analyses of as-received and aged electrode-coated membranes were performed with a TGA–FTIR system [i.e., a TGA TA 2050 (TA Instruments Co., USA) coupled to a Nicolet Nexus FTIR system (Thermo Nicolet Co., Madison WI)]. The samples were heated from 30 to 700°C at a constant rate of 10°C/min under a dry nitrogen atmosphere, and IR spectra were recorded in the spectral range of 4000–650 $cm^{-1}$ with a 4-$cm^{-1}$ resolution and 16 scans.

A Netzsch TG 209 F1 Iris simultaneous thermal analyzer, coupled to a Netzsch MS 403 Aëlos II quadruple mass spectrometer (Selb, Germany), was used for the TGA–mass spectrometry (MS) analysis. Two MS modes were used. The first one, called MS scan, proceeded to scan all masses between 5 and 300 with 0.1 s per $m/z$ value. The second MS mode, called MS selection, measured the response of up to 25 preselected fragments for 0.5–2 s. The experiments were performed on all membranes under a helium atmosphere at a heating rate of 10°C/min from 30 to 800°C. As an MS channetron is not a quantitative MS detector, the degradation products could not be quantified with high accuracy. Nevertheless, the magnitude of fragment formation could be evaluated from the integrated $m/z$ signal, and the values were compared between similar samples. The onset temperature of the degradation process ($T_{onset\text{-}TGA}$) and the last step degradation temperature ($T_{end\text{-}TGA}$) were extracted from either the derivative of the weight loss or MS data, as shown in Figure 1. The temperature width of thermal degradation ($\Delta T$) was defined as the difference between $T_{end\text{-}TGA}$ and $T_{onset\text{-}TGA}$.

### Wide-angle X-ray scattering (WAXS) experiments

WAXS diffractograms were recorded at the ambient temperature on a Bruker D8 Advance X-ray diffractometer (Karlsruhe, Germany) with Cu K$\alpha$ radiation ($\lambda$ = 1.5418 Å) in a reflection mode. Samples were analyzed in a rotation mode, and the diffraction scans were collected over a period of about 20 min from 4 to 90° (2$\theta$) with a scan increment of 0.02°.

### Water uptake measurements

Pieces of as-received and aged electrode-coated membranes were first dried at 70°C in desiccators for 24 h and weighed ($W_{dry}$). Then, the samples were stored at 70°C with 100% relative humidity for 24 h and weighed again ($W_{wet}$). The water uptake was determined at 25°C with the following equation:

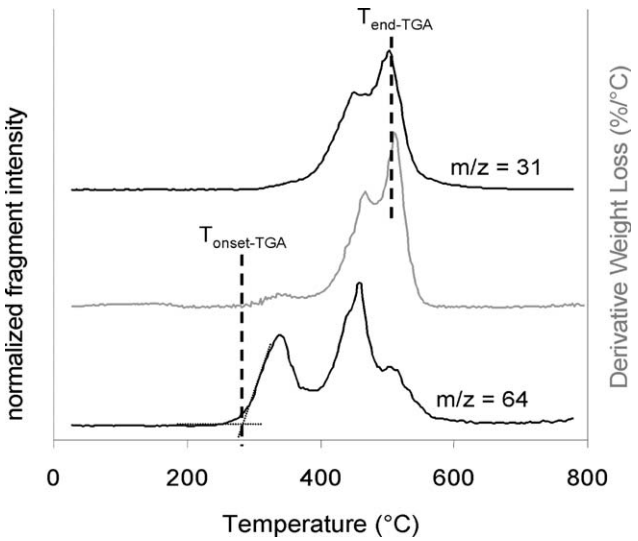


**Figure 1** Definition of the characteristic thermal degradation temperatures determined from the TGA and MS curves.[42]

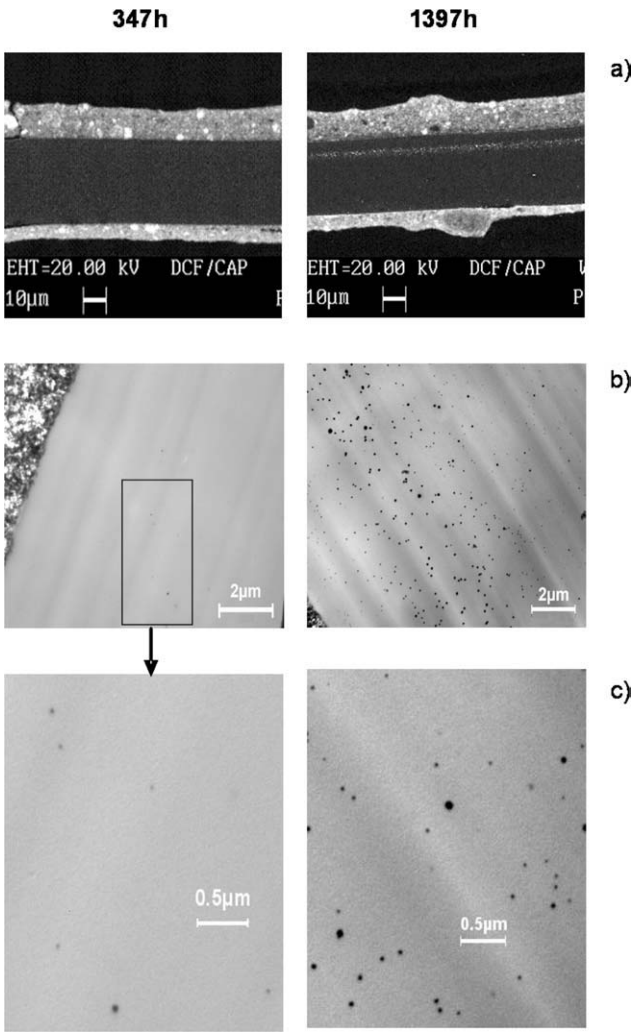


**Figure 2** (a) MEB and (b,c) TEM observations for the electrode-coated membranes after 347 and 1397 h.

$$\text{Water uptake} = \frac{W_{\text{wet}} - W_{\text{dry}}}{W_{\text{dry}}} \times 100 \qquad (1)$$

### Elemental analysis (EA)

EA of as-received and aged MEAs was carried out with a Rario EL III elemental analyzer (Elementar Analysensysteme GmbH, Hanau, Germany) from Central Analysis Service (USR-59, Centre National de la Recherche Scientifique, France). A custom-built potentiostat connected to a computer with an AD/DA converter was used to record cyclic voltammograms. EA was performed at least twice for each MEA.

### IEC

The IEC indicated the milliequivalents of $SO_3^-$ ions in 1 g of the dry polymer and thus could provide some indication of the number of accessible sulfonic sites. IEC values of as-received and aged electrode-coated membranes were determined as follows. Regenerated membranes were first soaked in a 2*M* NaCl solution to convert sulfonic acid groups into the sodium form. Then, the released $H^+$ was titrated with a 0.002*M* NaOH solution with a pH meter. The results were performed at least twice for each regenerated membrane.

### $^{19}$F-NMR experiments

Magic-angle-spinning NMR analyses were conducted on $^{19}$F nuclei at a resonance frequency of 376.498 MHz with a Bruker DSX-200 FT-NMR spectrometer. $^{19}$F-NMR spectra were acquired with a recycle delay of 3 s and a dwell time of 3 µs at 30 kHz after a tr–π–pulse–tr pulse sequence, which produced a rotation-synchronized Hahn spin echo.[25] The spectra for $^{19}$F were referenced to NaF, which was taken to be −221 ppm with respect to the more common standard $CFCl_3$. $^{19}$F-NMR spectra were performed on both electrode-coated membranes and nonregenerated membranes.

### FTIR measurements

Attenuated total reflection IR spectra were taken with a PerkinElmer Paragon 1000 FTIR spectrometer (Waltham, MA) equipped with a Pike Diamond Miracle attenuated total reflection device. Data in the 700–4000 $cm^{-1}$ frequency range were collected under a nitrogen gas flow for aged membranes dried at 70°C for at least 15 min. The symmetrical stretch band of the sulfonate group (dried $\nu_{SO_3^-}$) around 1060 $cm^{-1}$ was then determined for nonregenerated membranes.

## RESULTS AND DISCUSSION

### Macroscopic properties: membrane morphology and mechanical properties

On a macroscopic scale based on SEM observations, no defects such as voids or pinholes were detected within the membranes for the as-received and aged samples. Nevertheless, platinum particles in all the aged membranes, even for the shortest operating time examined (i.e., 347 h; Fig. 2), were detected. Consequently, in the membranes aged for 892 and 1497 h, the platinum band was observed on the SEM scale as a result of platinum dissolution and precipitation.[26–32] For every operation time, the polymer membrane thickness was measured from 10 SEM micrographs. The thickness results are reported in Figure 3. Within the measurement uncertainties, the membrane thickness exhibited a significant decrease

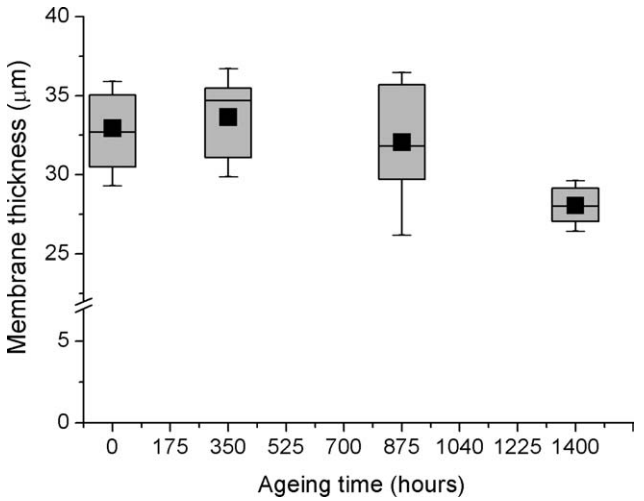


**Figure 3** Polymer membrane thickness as a function of the fuel-cell operation time.

upon aging from about 33 μm for the as-received sample to 28 μm for the longest aged specimen. This thinning effect became significant for aging times longer than 892 h. This decrease in the membrane thickness could have originated from the polymer erosion resulting from hydrogen peroxide attacks, as mentioned in the literature.[3,4] Nevertheless, a fraction of the membrane shrinkage could also result from some interchain crosslinking. An investigation of the tensile strength versus the aging time could also provide some information on the structural changes undergone by polymer membranes while aging. First, to detect possible anisotropy in the mechanical properties, the electrode-coated membranes were cut and tested along two orthogonal directions, that is, the tensile test axis parallel to the length and width of the MEA. Figure 4 shows stress–strain curves of the as-received specimens. The sample tested with the main axis along the MEA width

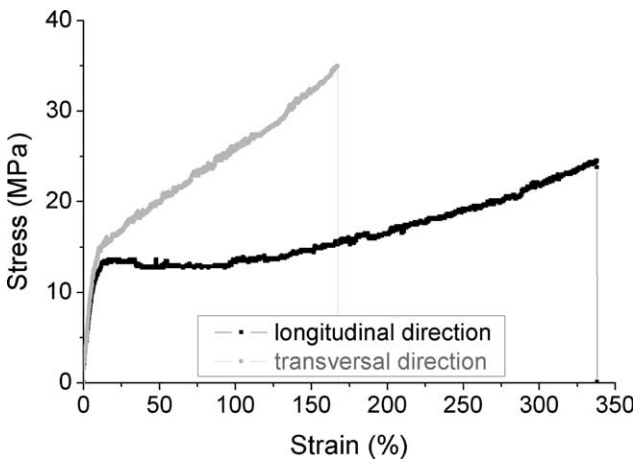


**Figure 4** Tensile test curves for the as-received samples tested along the transversal and longitudinal directions of the electrode-coated membranes.

**TABLE I**
**Mechanical Characteristics of the Electrode-Coated Membranes After Fuel-Cell Operation**

| Aging time (h) | Young's modulus (MPa) | Stress at break (MPa) | Strain at break (%) |
|---|---|---|---|
| 0 | 168 ± 8 | 38 ± 2 | 194 ± 8 |
| 347 | 193 ± 6 | 44 ± 4 | 139 ± 16 |
| 892 | 187 ± 4 | 41 ± 5 | 136 ± 20 |
| 1397 | 223 ± 11 | 47 ± 4 | 120 ± 14 |

exhibited higher stiffness associated with both an increase in the yield stress and a decrease in the strain at break. This provided evidence for mechanical anisotropy that was probably due to the membrane extrusion process.

In the rest of the article, the mechanical properties of the membranes are discussed with respect to samples whose main axis strength was parallel to the width of the MEAs. Values of $E$ and the stress and strain at break for the different aging times are given in Table I. With increasing aging time, $E$ and the stress at break tended to increase from 168 and 38 MPa to 223 and 47 MPa, respectively, for the longest aged sample, whereas the strain at break tended to decrease from 200 to 120%. From these results, it can be concluded that the ductile behavior of the polymer membrane tended to decrease with long aging times under normal service conditions. These observations are consistent with the observations of Luo et al.,[20] who reported a slight decrease in the breaking strength accompanied by an increase in the yield stress for MEAs aged within a laboratory stack. The decrease in the ductile behavior undergone by the polymer membrane could have originated from a decrease in the hydration ability of the membrane on aging, as reported in the literature,[33,34] or from the formation of a randomly crosslinked polymer network[22] due to polymer chain scission and subsequent random interchain crosslinking. Both hypotheses are also consistent with the decrease in the water uptake from 22% for the as-received membrane to 10% for the longest aged sample. This could have resulted from a decrease in the side chains' ability to promote swelling with water molecules due to a chemical degradation of the accessible sulfonic groups by a specific attack or crosslink reaction.

## Changes in the thermal behavior

The effect of aging on the polyelectrolyte was further studied with DMA. In addition to the viscoelastic characteristics, DMTA can provide information on the polymer microstructure in terms of the molecular mobility of the macromolecular chains. Plots of tan δ and log $E'$ at 1 Hz versus the temperature are

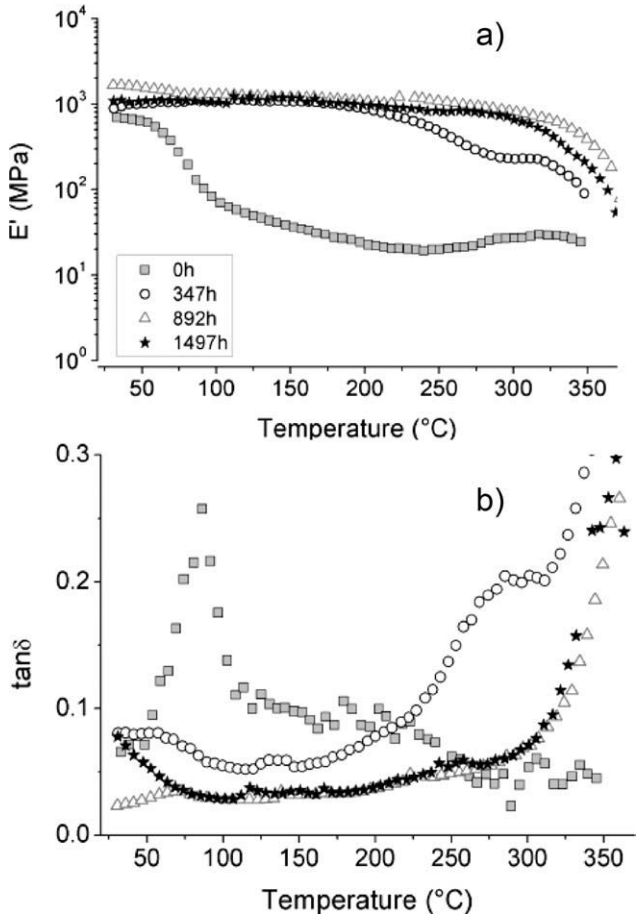


**Figure 5** Plots of (a) log $E'$ and (b) tan δ versus the temperature at 1 Hz for the as-received and aged electrode-coated membranes.

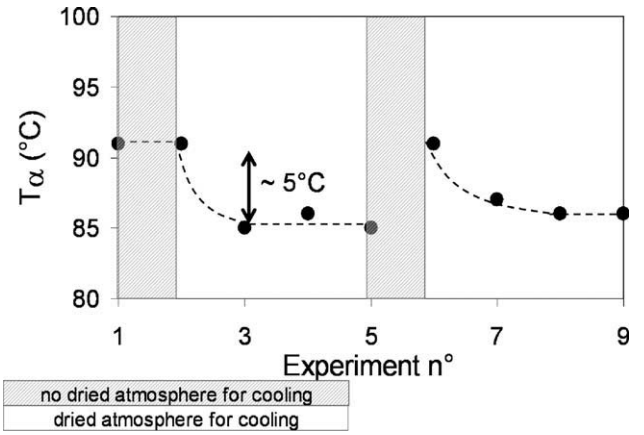


**Figure 6** $T_\alpha$ (1 Hz) dependence of the experiments from 30 to 120°C for the as-received sample. These experiments were performed under a nitrogen flow even for cooling except after experiments 1 and 5.

shown in Figure 5 for the as-received and aged electrode-coated membranes.

With the temperature increasing from the ambient temperature to 400°C, the following two transitions could be detected for the as-received sample. The α transition, located at about 90°C (1 Hz), was characterized by a well-defined tan δ peak accompanied by a drop in $E'$. The temperature of this transition belonged to the large temperature range in the literature (67[35] to 117[36]) reported for PFSA membranes with an IEC of 0.9. Assuming the Arrhenius law, we calculated the activation energy from the tan δ peak locations to be close to 500 kJ/mol. The pre-exponential factor was around $10^{65}$ Hz, which was much larger than the Debye frequency. These data suggested that the α relaxation displayed by the as-received sample originated from correlated motions usually related to the glass transition. According to the literature,[37–39] these correlated motions concern the ionic domains, and $T_\alpha$ was slightly dependent on the water content of the membrane as a 5°C decrease was observed after heating up to 120°C (Fig. 6). At higher temperatures, a slight and irreversible increase in log $E'$ from 275°C was followed by a slight decrease at temperatures above 325°C. Because of measurement uncertainties, no tan δ peak was detected. These changes in $E'$ versus the temperature were not frequency-dependent. In this temperature range, thermal degradation of the polymer occurred.[40–42] It can be suggested that this behavior resulted in some successive chain scission/recombination/scission with increasing temperature.[43]

Fuel-cell operation led to two apparently independent changes in the dynamic mechanical behavior of the membrane (Fig. 5 and Table II).

First, there was an increase in $E'$ over the entire analyzed temperature range. This was consistent with previous results from tensile tests

**TABLE II**
**Characteristic Temperatures[a] of the Electrode-Coated Membrane from the DMTA and TGA–MS Experiments**

| Operating time (h) | $T_\alpha$ (°C) | $T_{onset\text{-}DMTA}$ (°C) | $T_{onset\text{-}TGA}$ (°C) | $T_{end\text{-}TGA}$ (°C) | $\Delta T$ | Dried $\nu_{SO_3^-}$ ($cm^{-1}$) |
|---|---|---|---|---|---|---|
| 0 | 90 | 65 | 280 | 490 | 210 | 1061 |
| 347 | 295 | 220 | 400 | 485 | 85 | 1071 |
| 892 | Not detected | 310 | 400 | 490 | 90 | 1072 |
| 1397 | Not detected | 330 | 400 | 490 | 90 | 1071 |

[a] The accuracy of the temperatures was 5°C.
The FTIR $\nu_{SO_3^-}$ wave number in the dried state was also reported for the membrane with an accuracy of 1 $cm^{-1}$.

**TABLE III**
**Assignments of the *m/z* Ions and Their Relative Intensity Signals for Some Interesting Products Involved in the Degradation of the Electrode-Coated Membrane**

| Gas molecule | Main *m/z* | Relative intensity of the main fragment | Fragment | Associated signal | IR detection |
|---|---|---|---|---|---|
| $H_2O$ | 18 | 95 | $H_2O^+$ | | Yes |
| HF | 19 | >100 | $F^+$ | | Yes |
| $CO_2$ | 44 | 70 | $CO_2^+$ | 28 | Yes |
| $C_2F_4$ (mainly), $C_xF_y$ | 31 | 100 | $CF^+$ | 50, 62, 68, 69, 74, 93, 81, 100, 150 | Yes |
| $COF_2$ | 47 | 13 | $CFO^+$ | 66 | No |
| $SO_2$ | 64 | 25 | $SO_2^+$ | 32, 48 | No in aged membrane |
| Perfluorether | 85 | 0.7 | $CF_3O^+$ | 28 | No |
| $SOF_2$ | 86 | 0.6 | $SOF_2^+$ | 67 | No |
| Perfluoroketone | 97 | 4 | $C_2F_3O^+$ | 119 | No |

measurements that showed an increase in the stiffness of the membrane on aging. Among the aged samples, only the 347h-aged sample displayed a tan δ peak as a shoulder located at about 295°C at 1 Hz, and this was accompanied by a decrease in $E'$. This mechanical relaxation showed a frequency dependence similar to the α relaxation related to the glass-transition temperature ($T_g$) displayed by the fresh sample. The apparent activation energy and pre-exponential factor values determined from the Arrhenius law were about 500 kJ/mol and $10^{70}$ Hz, respectively. These values were close to those displayed by the α relaxation of the as-received specimen.

Then, with respect to the fresh specimen behavior, a 200°C increase in the main temperature was evidenced. For the longest aged samples, $E'$ even lost its frequency dependence. Accordingly, this transition could not be related to the polymer glass transition but was instead assigned to the onset of the thermal degradation of the polymer. This was confirmed by TGA in air. This could mean that for long service durations, the molecular mobility was so hindered that $T_g$ was increased up to temperatures beyond the onset of the temperature degradation. This phenomenon is commonly observed for thermoset polymers showing a high molecular crosslinking degree. Accordingly, the overall increase in $E'$, accompanied by a strong $T_g$ shift toward higher temperatures, seems consistent with the formation of a compact polymer network due to chemical crosslinking between polymer chains. This hypothesis is consistent with the WAXS amorphous pattern displayed by the membrane.

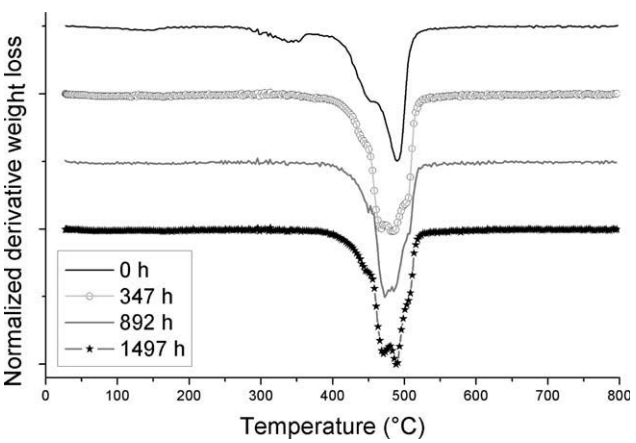


**Figure 7** Derivative weight loss curves versus the temperature for the as-received and aged MEAs.

To obtain more knowledge about the structural changes undergone by the polymer membrane on aging that gave rise to drastic changes in the thickness and mechanical properties, the thermal stability was investigated by TGA coupled with IR spectrophotometry (TGA–FTIR) or MS (TGA–MS). The identification of the gases that evolved during the thermal process should help us to understand structural changes within the polymer. As described in a previous TGA–MS study,[42] a first heating scan was performed on the electrode-coated membrane with the *m/z* scan mode to identify the key fragments and their corresponding mass numbers from MS analysis. As for $H^+$-form Nafion,[42] different fragment groups were detected and are reported in Table III. Figure 7 displays derivatives of curves of the mass loss versus temperature recorded on heating at 10°C/min from TGA for as-received and aged samples. The corresponding MS graphs for the selected *m/z* signal, that is, for the selected key fragments, are also shown in Figure 8. The changes in the thermal decomposition under an inert atmosphere upon aging were clearer from the fragment signals than from TG derivative curves (Figs. 7 and 8). These analyses showed some interesting results:

- The MS signal presented a much better resolution than that obtained with IR. For instance, the TGA–FTIR experiments did not permit the detection of $SO_2$ gas for aged samples as

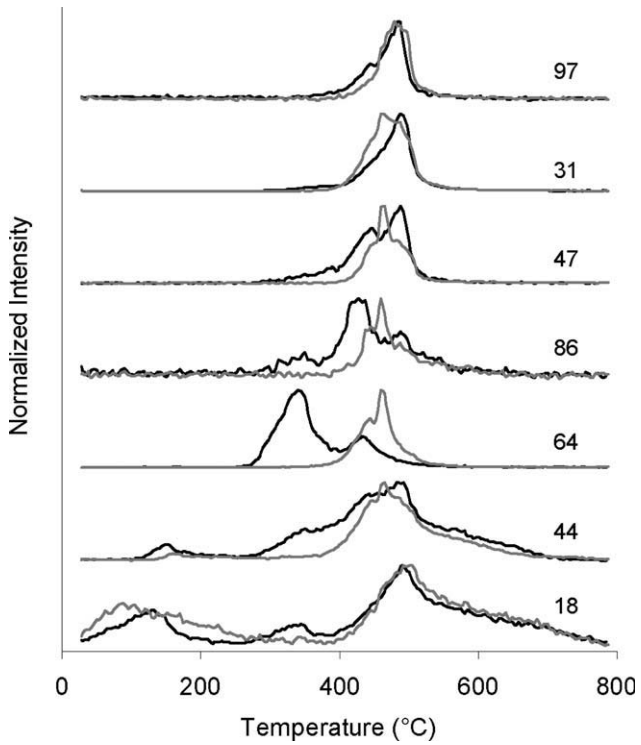


**Figure 8** Normalized MS graphs for the as-received (black) and aged (gray) electrode-coated membranes. Selected $m/z$ values are given.

characteristic sulfur dioxide gas absorption bands[44] overlapped those of tetrafluoroethylene gas.[44]

- The TGA–MS signals of the as-received MEA were in agreement with the three-step membrane decomposition,[40,41] that is, the degradation of the functional group with the formation of sulfur dioxide ($m/z = 64$), the degradation of lateral chains involving the formation of both carbonyl fluoride ($m/z = 47$) and thionyl fluoride ($m/z = 867$), and the main-chain degradation with the detection of perfluorocarbon groups ($m/z = 31$).
- All the aged electrode-coated membranes displayed the same TGA–MS signal, which was different from that of the as-received MEA.
- All the selected fragments related to the degradation of lateral chains ($m/z = 64$ and 86) were shifted by operation toward higher temperatures. Therefore, aging seemed to induce an improvement in the thermal stability of the side chains. Moreover, the thermal stability of the main backbone chain was less affected by the life test duration ($m/z = 31$ and 97); the fragment temperature was indeed independent of the aging time.
- These changes with aging were also observed for uncoated membranes (as for the DMTA experiments) and thus could not be attributed to a catalyst layer effect.

Therefore, the enhancement of the thermal stability of the side chains induced by aging could originate (1) from some chemical crosslinking leading to —($SO_2$—O—$SO_2$)— bridges connecting neighboring chains, (2) from ionic crosslinking involving the presence of cationic contaminants and yielding to the formation of bridges (—$SO_3^-Mn^+SO_3^-$—) between neighboring chains, or (3) from a partial desulfonation of the membrane leading to —($CF_2$—$SO_2$—$CF_2$)— bridges. These conclusions are consistent with aforementioned assumptions concerning the possible origins of the modifications of the macroscopic properties undergone by the polymer membrane on aging. However, this last hypothesis could not be confirmed or ruled out by $m/z = 64$ MS intensities because the MS detector did not permit a quantitative analysis. Nevertheless, it showed that aging the membrane induced the changes in the sulfonic species environment leading to the thermal stability of the side chain and the drastic changes in the mechanical behavior and hydration ability. To identify the key structural changes in the polymer membrane on aging, additional chemical investigations were carried out.

### Membrane chemical degradations induced by aging

The contents of sulfur and fluorine atoms, evaluated by EA, are listed for the as-received and aged MEAs in Table IV. The sulfur and fluorine contents in the MEAs remained unchanged with the operating time. On the basis of these results, the partial

**TABLE IV**
**Chemical Analysis Results for the MEA or Membrane**

| Operating time (h) | MEA | | IEC after the acid treatment for the membrane (mequiv/g) | [c,f,e]/[a′,a″,g] area ratio for the MEA and membrane |
|---|---|---|---|---|
| | S (wt %) | F (wt %) | | |
| 0 | 2.8 ± 0.3 | 50 ± 2 | 0.84 ± 0.02 | 0.266 ± 0.001 |
| 347 | 2.9 ± 0.4 | 51 ± 2 | 0.88 ± 0.02 | 0.265 |
| 892 | 2.9 ± 0.1 | 49 ± 1 | 0.83 ± 0.02 | 0.266 |
| 1397 | 3.0 ± 0.5 | 52 ± 3 | 0.84 ± 0.02 | 0.264 ± 0.004 |

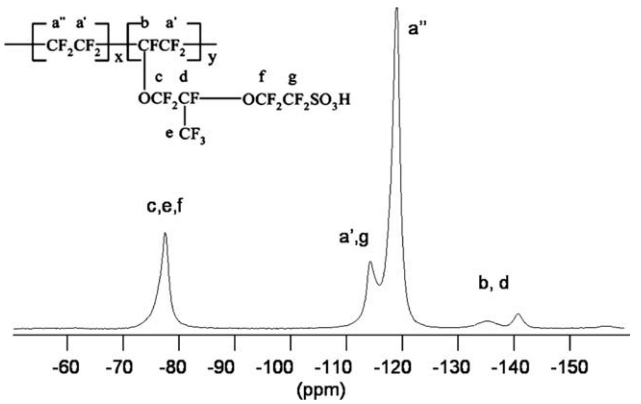


**Figure 9** $^{19}$F-NMR spectra of the MEA samples. The symbols refer to the locations of corresponding fluorine atoms in the chemical structure of Nafion.

desulfonation of the membrane and —($CF_2$—$SO_2$—$CF_2$)— bridge hypotheses could be excluded. Moreover, FTIR experiments with the membranes confirmed that no absorption band in the 1400–1500 $cm^{-1}$ wave-number range associated with S—O—S bridges[9,23,24,45] was detected. $^{19}$F-NMR spectra were taken for the as-received and aged MEAs (Fig. 9). For all samples, five $^{19}$F-NMR resonances were observed at about −140, −136, −119, −114, and −78 ppm, and these were assigned to side-chain CF (d), backbone CF (b), $(CF_2)_n$ (a″), $CF_2$ bonded to an $SO_3^-$ group and $CF_2$ attached to CF within the backbone (a′ and g), and $CF_3/OCF_2$ groups (d, e, and c), respectively.[25,46] Aging did not induce significant changes in the overall pattern of $^{19}$F-NMR spectra displayed by the samples. The integrated values of $^{19}$F-NMR peaks for the MEAs and

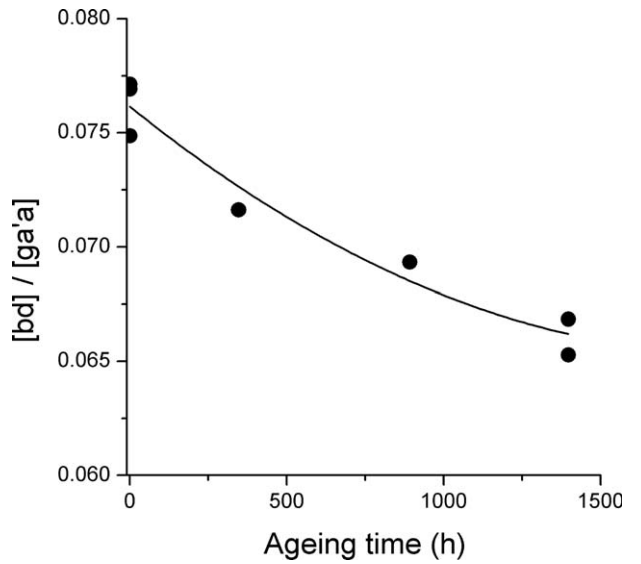


**Figure 10** Change in the $^{19}F_{b,d}$-NMR integrated values with the operating fuel-cell time.

**TABLE V**
**Carbon-Fluorine Bond Dissociation Energies ($E_{C\text{-}F}$) for the Perfluorinated Model Compounds Calculated by Mitov et al.[47]**

| Model compound | $E_{C—F}$ (kJ/mol) |
|---|---|
| $CF_3$—$CF_2$—$CF_2$—F | 478 |
| $CF_3$—$CF_2$—CF(—F)—$CF_2$—$CF_3$ | 433 |
| $CF_3$—$CF_2$—$CCF_3$(—F)—$CF_2$—$CF_3$ | 386 |

membranes were estimated. The peak area ratio of the [c,f,e] signal to the [a′,a″,g] resonance remained constant with the duration test life and equal to 0.265 ± 0.002. In contrast, the integrated value of the [b,d] resonances progressively decreased with respect to both the [c,f,e] and [a′,a″,g] peak areas (Fig. 10), whereas the intensity ratio between b and d peaks remained almost constant and equal to about 0.85 ± 0.03, regardless of the aging time. This set of data suggests that a 10% loss in d and b fluorine occurred, leading to a decrease in the fluorine weight content of less than 0.5%, which could not be detected by EA. This loss could not be attributed to degradation taking place in the side chains as the [c,f,e] to [a′,a″,g] ratio remained constant. It can be suggested that CF groups were attacked by a radical, and this led to a quaternary carbon radical. This result is supported by the C—F dissociation energies reported in Table V,[47] which suggest that tertiary C—F bonds were the less stable positions on the perfluorinated chain.[2] This covalent reticulation implied less than 1% carbon and could not be solely responsible for the drastic changes in the thermal behavior. In addition, FTIR spectra did not reveal —($SO_2$—O—$SO_2$)— at 1440 $cm^{-1}$,[22,24,48] or carboxylic function at 1813 and 1775 $cm^{-1}$.[49] Finally, the last hypothesis, (ionic crosslinking) was not excluded as $^{19}$F-NMR is not sensitive to cationic exchange.

## Analysis of the regenerated membrane

It is now of interest to investigate the presence of cationic contaminants within the polymer that could give rise to the formation of ionic crosslinking networks. This structural evolution upon aging could

**TABLE VI**
**Characteristic Temperatures[a] (°C) of the Regenerated Membrane from DMTA and TGA–MS Experiments**

| Operating time (h) | $T_{onset\text{-}DMTA}$ | $T_{onset\text{-}TGA}$ | $\Delta T$ |
|---|---|---|---|
| 0 | 90 | 270 | 235 |
| 347 | 95 | — | — |
| 892 | 90 | 260 | 250 |
| 1397 | 90 | — | — |

[a] The accuracy of the temperatures was 5°C.

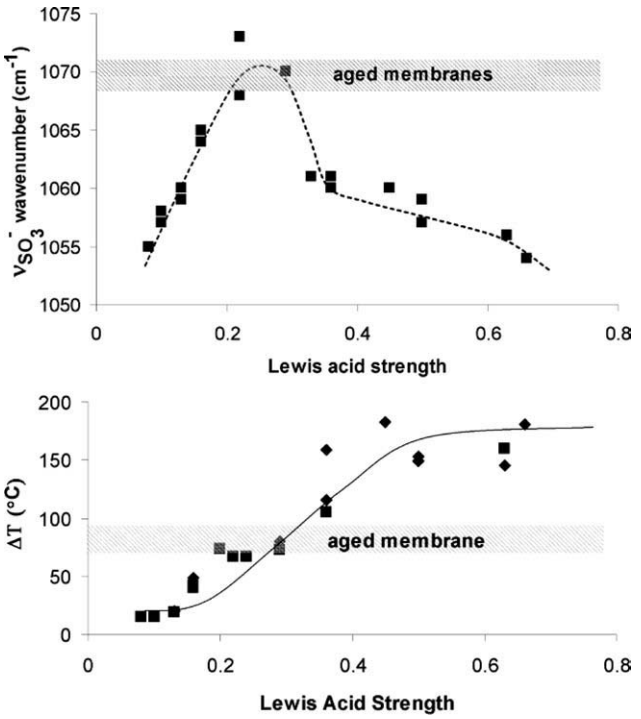


**Figure 11** Characteristic parameters of the aged membranes superimposed on calibration curves from the TGA and FTIR measurements.[42]

indeed explain the aforementioned changes in the properties[42] and would not require altering the number of sulfonate groups, as confirmed by IEC determined for the regenerated membrane (Table IV).

To reveal this plausible ionic crosslinking, membranes extracted from aged MEAs were regenerated with an acid treatment and characterized with DMA and TGA–MS.

The temperature onsets of the drop modulus ($T_{onset\text{-}DMTA}$) for the regenerated membranes are listed in Table VI and can be compared to those before regeneration (Table II). With respect to the behavior observed with nonregenerated aged samples, a strong shift of $T_{onset\text{-}DMTA}$ toward lower temperatures revealed the reversibility of the aging process when they were soaked in acidic solutions. The onset temperature of the $E'$ drop exhibited by the regenerated aged samples tended to be close to that of the fresh samples, regenerated and nonregenerated. Moreover, this transition displayed by the regenerated membranes recovered a frequency dependence, regardless of the aging time and even for the longest duration test.

In addition, the patterns of the TGA–MS graphs displayed by the regenerated aged membranes were the same as those exhibited by these samples before the acid treatment. As for the unaged MEA, the degradation of side chains in the regenerated aged membranes resulted in two-step $SO_2$ formation. The characteristic parameters extracted from the TGA–MS experiments with regenerated membranes (Table VI) were close to those determined for the as-received MEA (Table II). The thermal shift observed in the aged MEA thus resulted from chemical modifications, which were reversible with acid treatments. This acid treatment reversibility was demonstrated for the decondensation of sulfonic anhydride into sulfonic acids.[48] Nevertheless, this hypothesis was excluded by FTIR. We can conclude that these thermal shifts resulted from cationic pollution induced by the fuel-cell operation. This pollution led to ionic crosslinking of sulfonic moieties. To identify the cation at the origin of this pollution, we report data for an aged MEA in TGA–MS and FTIR calibration curves based on the Lewis acid strength (LAS) of cations.[42] The graphs in Figure 11 clearly show that the characteristics of the aged membrane from both TGA and FTIR measurements were related to cations with an LAS ranging from 0.2 to 0.3. This LAS found for the aged membrane was close to the Lewis basic strength of sulfonate groups in Nafion.[42,50] As a result, the contaminated cation exhibited a strong affinity to the functional group of the PFSA membrane.

## CONCLUSIONS

To better understand the key parameters governing the durability of PEFMCs under actual service conditions, a large series of electrode-coated membranes aged for different fuel-cell operations were investigated. With aging, changes in the morphology, hydration ability, macroscopic mechanical properties, viscoelastic behavior, and thermal properties were revealed by SEM, water uptake measurements, tensile tests, DMTA, and TGA–MS. Chemical degradation of the membranes induced by aging was investigated with $^{19}$F-NMR, EA, and IEC measurements. To detect the presence of cationic contamination, the thermal behavior of all regenerated membranes was in turn investigated.

The key features yielding to changes in the membranes properties with aging can be described as follows:

- In our systems, the membrane was contaminated in the earlier stage of fuel-cell operation. This resulted in thermal stabilization of the membrane. $T_\alpha$ was shifted toward higher temperatures because of the formation of the reversible ionic network. This network formation also affected the mechanical properties of the MEA at room temperature. The cationic contamination of the membrane implied a large decrease in the water content (a ratio of 2). These cations had an LAS of about 0.25 and strongly

interacted with the sulfonate moieties of Nafion.[42] The LAS value range suggests that they could be $Ba^{2+}$, $Sr^{2+}$, or $Ca^{2+}$.[51] Although the origin of these cations remains unclear, their presence was partially confirmed by analytical analysis.

- In the earlier stage of fuel-cell operation, platinum particles were formed in the membrane, giving rise to the platinum band at 900 h. However, the macroscopic properties may in no way have resulted from a mechanical reinforcement phenomenon as the regenerated MEA still contained these particles and lost the reinforcement.
- In addition, even after only 400-h fuel-cell operation, NMR experiments suggested some chemical degradation process leading to a small loss of fluorine atoms on tertiary carbons supported by C—F bond energies. This, in turn, might imply some covalent crosslinking. To the best of our knowledge, this is reported here for the first time; moreover, this fluorine loss was deduced from NMR data without any hypothesis about the chemical structure of the membrane. However, no impact of these reticulations could be detected on the membrane properties because of the low carbon fraction involved.
- Finally, the chemical degradation of the membrane, reported as an unzipping process, was revealed by the thickness decrease and began at 900 h; this matched the platinum band formation. Even so, as the membrane was polluted by cations, both the diffusion of water and the ionic conductivity of the membrane were significantly reduced.[52–57] Therefore, it could be not excluded that it involved higher kinetics of the chemical degradation of the membrane due to a peroxide radical attack.

The authors thank one of their students, Laetitia Reymond, for her analysis of the regenerated membranes.

## References


1. Collier, A.; Wang, H.; Yuan, X. Z.; Zhang, J.; Wilkinson, D. P. Int J Hydrogen Energy 2006, 31, 1838.
2. Schiraldi, D. A. Polym Rev 2006, 46, 315.
3. Xie, T.; Hayden, C. A.; Healy, J.; Olson, K. Advances in Materials for Proton Exchange Membrane Fuel Cell Systems; Brooks/Cole: Pacific Grove, CA, 2005; p 24.
4. Xie, T.; Hayden, C. A. Polymer 2007, 48, 5497.
5. Inaba, M.; Kinumoto, T.; Kiriake, M.; Umebayashi, R.; Tasaka, A.; Ogumi, Z. Electrochim Acta 2006, 51, 5746.
6. Tang, H.; Peikang, S.; Jiang, S. P.; Wang, F.; Pan, M. J Power Sources 2007, 170, 85.
7. Merlo, L.; Ghielmi, A.; Cirillo, L.; Gebert, M.; Arcella, V. J Power Sources 2007, 171, 140.
8. Aoki, M.; Uchida, H.; Watanabe, M. Electrochem Commun 2006, 8, 1509.
9. Kinumoto, T.; Inaba, M.; Nakayama, Y.; Ogata, K.; Umebayashi, R.; Tasaka, A.; Iriyama, Y.; Abe, T.; Ogumi, Z. J Power Sources 2006, 158, 1222.
10. Mittal, V. O.; Kunz, H. R.; Fenton, J. M. J Electrochem Soc 2007, 154, B652.
11. Teranishi, K.; Kawata, K.; Tsushima, S.; Hirai, S. Electrochem Solid-State Lett 2006, 9, A475.
12. Jian, X.; David, L. W., III; David, M. W.; Thomas, A. Z.; Plamen, A.; Rodney, L. B. J Electrochem Soc 2005, 152, A104.
13. Healy, J.; Hayden, C.; Xie, T.; Olson, K.; Waldo, R.; Brundage, M.; Gasteiger, H.; Abbott, J. Fuel Cells 2005, 5, 302.
14. Xie, J.; Wood, D. L.; Wayne, D. M.; Zawodzinski, T. A.; Atanassov, P.; Borupa, R. L. J Electrochem Soc 2005, 152, A104.
15. Stucki, S.; Scherer, G. G.; Schlagowski, S.; Fischer, E. J Appl Electrochem 1998, 28, 1041.
16. Pozio, A.; Silva, R. F.; De Francesco, M.; Giorgi, L. Electrochim Acta 2003, 48, 1543.
17. Panchenko, A.; Dilger, H.; Kerres, J.; Hein, M.; Ullrich, A.; Kaz, T.; Roduner, E. Phys Chem Chem Phys 2004, 6, 2891.
18. Fowler, M. Presented at Fuel Cell Technology Day, Kingston, Ontario, Canada, 2007.
19. Yu, J.; Matsuura, T.; Yoshikawa, Y.; Islam, M. N.; Hori, M. Phys Chem Chem Phys 2005, 7, 373.
20. Luo, Z.; Li, D.; Tang, H.; Pan, M.; Ruan, R. Int J Hydrogen Energy 2006, 31, 1831.
21. Ghassemzadeh, L.; Marrony, M.; Barrera, R.; Kreuer, K. D.; Maier, J.; Müller, K. J Power Sources 2009, 186, 334.
22. Qiao, J.; Saito, M.; Hayamizu, K.; Okada, T. J Electrochem Soc 2006, 153, A967.
23. Chen, C.; Levitin, G.; Hess, D. W.; Fuller, T. F. J Power Sources 2007, 169, 288.
24. Collette, F. M.; Lorentz, C.; Gebel, G.; Thominette, F. J Membr Sci 2009, 330, 21.
25. Chen, Q.; Schmidt-Rohr, K. Macromolecules 2004, 37, 5995.
26. Yasuda, K.; Taniguchi, A.; Akita, T.; Ioroi, T.; Siroma, Z. Phys Chem Chem Phys 2006, 8, 746.
27. Akita, T.; Taniguchi, A.; Maekawa, J.; Siroma, Z.; Tanaka, K.; Kohyama, M.; Yasuda, K. J Power Sources 2006, 159, 461.
28. Guilminot, E.; Corcella, A.; Charlot, F.; Maillard, F.; Chatenet, M. J Electrochem Soc 2007, 154, B96.
29. Danérol, A.-S. Ph.D. Dissertation, Université de Savoie: Le Bourget du Lac, France, 2008.
30. Bi, W.; Gray, G. E.; Fuller, T. F. Electrochem Solid-State Lett 2007, 10, B101.
31. Kim, L.; Chung, C. G.; Sung, Y. W.; Chung, J. S. J Power Sources 2008, 183, 524.
32. Ohma, A.; Yamamoto, S.; Shinohara, K. J Power Sources 2008, 182, 39.
33. Huang, X.; Solasi, R.; Zou, Y.; Feshler, M.; Reifsnider, K.; Condit, D.; Burlatsky, S.; Madden, T. J Polym Sci Part B: Polym Phys 2006, 44, 2346.
34. Tang, Y.; Karlsson, A. M.; Santare, M. H.; Gilbert, M.; Cleghorn, S.; Johnson, W. B. Mater Sci Eng A 2006, 425, 297.
35. Ghielmi, A.; Vaccarono, P.; Troglia, C.; Arcella, V. J Power Sources 2005, 145, 108.
36. Grava, W. M.; Okada, T.; Kawano, Y. J Therm Anal Calorim 2007, 89, 163.
37. Kyu, T.; Hashiyama, M.; Eisenberg, A. Can J Chem 1983, 61, 680.
38. Bauer, F.; Denneler, S.; Willert-Porada, M. J Polym Sci Part B: Polym Phys 2005, 43, 786.
39. Page, K. A.; Cable, K. M.; Moore, R. B. Macromolecules 2005, 38, 6472.
40. Wilkie, C. A.; Thomsen, J. R.; Mittleman, M. L. J Appl Polym Sci 1991, 42, 901.
41. Samms, S. R.; Wasmus, S.; Savinell, R. F. J Electrochem Soc 1996, 143, 1498.

42. Bas, C.; Reymond, L.; Danérol, A.-S.; Albérola, N. D.; Rossinot, E.; Flandin, L. J Polym Sci Part B: Polym Phys 2009, 47, 1381.
43. Lesueur, D.; Albérola, N. D. Synth Met 1997, 88, 133.
44. Smith, A. L. The Coblentz Society Desk Book of Infrared Spectra, 2nd ed.; The Coblentz Society: Kirkwood, MO, 1982.
45. Alentiev, A.; Kostina, J.; Bondarenko, G.; Desalination 2006, 200, 32.
46. Takasaki, M.; Kimura, K.; Kawaguchi, K.; Abe, A.; Katagiri, G. Macromolecules 2005, 38, 6031.
47. Mitov, S.; Panchenko, A.; Roduner, E. Chem Phys Lett 2005, 402, 485.
48. Collette, F. Ph.D. Dissertation, ENSAM Paris, 2008.
49. Pianca, M.; Barchiesi, E.; Esposto, G.; Radice, S. J Fluorine Chem 1999, 95, 71.
50. Quezado, S.; Kwak, J. C. T.; Falk, M. Can J Chem 1984, 62, 958.
51. Brown, I. D. In Structure and Bonding in Crystals; O'Keffe, M.; Navrotsky, A., Eds.; Academic: New York, 1981; p 1.
52. Yeager, H. L.; Steck, A. J Electrochem Soc 1981, 128, 1880.
53. Legras, M.; Hirata, Y.; Nguyen, Q. T.; Langevin, D.; Metayer, M. Desalination 2002, 147, 351.
54. Suresh, G.; Sodaye, S.; Scindia, Y. M.; Pandey, A. K.; Goswami, A. Electrochim Acta 2007, 52, 5968.
55. Okada, T.; Ayato, Y.; Yuasa, M.; Sekine, I. J Phys Chem B 1999, 103, 3315.
56. Kelly, M. J.; Fafilek, G.; Besenhard, J. O.; Kronberger, H.; Nauer, G. E. J Power Sources 2005, 145, 249.
57. Wang, H.; Turner, J. A. J Power Sources 2008, 183, 576.